ELSEVIER

Chemical Engineering Journal 143 (2008) 43–50

Chemical Engineering Journal

www.elsevier.com/locate/cej

Adsorption behaviors of Congo red on the *N*,*O*-carboxymethyl-chitosan/montmorillonite nanocomposite

Li Wang [a,b], Aiqin Wang [a,*]

[a] *Center of Eco-material and Green Chemistry, Lanzhou Institute of Chemical Physics, Chinese Academy of Sciences, Lanzhou 730000, PR China*

[b] *Graduate School of the Chinese Academy of Sciences, Beijing 100049, PR China*

Received 1 December 2006; received in revised form 20 February 2007; accepted 9 December 2007

Abstract

A series of *N*,*O*-carboxymethyl-chitosan/montmorillonite (*N*,*O*-CMC–MMT) nanocomposites were prepared by controlling the molar ratios of *N*,*O*-carboxymethyl-chitosan (*N*,*O*-CMC) and montmorillonite (MMT). The nanocomposites were characterized by FTIR, XRD and SEM. Adsorption of Congo red (CR) anionic dye from aqueous solution onto *N*,*O*-CMC–MMT was studied. The results showed that the nanocomposite with the molar ratio of *N*,*O*-CMC to MMT of 5:1 exhibited the higher adsorption capacity. This may be attributed to the fact that the introduction of *N*,*O*-CMC in the galleries of MMT may have different influences on physico-chemical properties of MMT and in turn result in different influences on adsorption capacity of *N*,*O*-CMC–MMT for CR. The effects of different molar ratios of *N*,*O*-CMC and MMT, initial pH value of the dye solution and temperature on adsorption capacities of samples for CR dye have been investigated. The results of adsorption behaviors of CR on *N*,*O*-CMC–MMT indicated that all the adsorption processes followed the pseudo-second-order and the Langmuir isotherm, respectively.

Keywords: *N*,*O*-Carboxymethyl-chitosan; Nanocomposite; Congo red; Adsorption; Kinetic

1. Introduction

Water contamination resulting from dyeing and finishing in textile industry is a major concern. Discharging large amount of dyes in water resources accompanied with organics, bleaches, and salts can affect the physico-chemical properties of freshwater. In addition to their unwanted colors, some of these dyes may degrade to produce carcinogens and toxic products [1]. Hence, the removal of dyes from waste effluents becomes environmentally important.

It is rather difficult to treat dye effluents because of their synthetic origins and their mainly aromatic structure, which are biologically non-degradable [2]. Several methods are available for color removal from wastewater such as membrane separation, aerobic and anaerobic degradation using various microorganisms, chemical oxidation, coagulation and flocculation, adsorption using different kinds of adsorbents [3,4]. Among them, adsorption is generally considered to be an effective method for quickly lowering the concentration of dissolved dyes in an effluent [5]. Up to now, many low-cost adsorbents have been tested on the possibility to lower dye concentrations from aqueous solutions, such as orange peel [6], acid-activated red mud [7], fly ash [8,9] and others [10–15]. However, the low-cost adsorbents for Congo red (CR) dye often have low adsorption capacities. Therefore, to improve adsorption performance, new adsorbents are still under development.

Chitosan (CTS) has been reported with the high potential for the adsorption of anionic dyes [16–18] since the amino ($-NH_2$) and hydroxyl (–OH) groups on CTS chains can serve as electrostatic interaction and coordination sites, respectively [19]. Generally, in order to improve the mechanical properties and specific gravity of CTS and further enhance the adsorption capacity of CTS for dye, the surface of CTS is modified by a suitable approach. Various studies were conducted to make derivatives of CTS by chemical modification techniques, such as PEG-grafting, sulfonation, quaternarization [20], *N*- and *O*-

* Corresponding author. Tel.: +86 931 4968118; fax: +86 931 8277088.
E-mail address: aqwang@lzb.ac.cn (A. Wang).

1385-8947/$ – see front matter © 2007 Elsevier B.V. All rights reserved.
doi:10.1016/j.cej.2007.12.007

hydroxylation and carboxymethylation-chitosan (CMC) [21]. Among the derivatives, CMC is an amphiprotic ether derivatives, which contains active hydroxyl (–OH), carboxyl (–COOH) and amine ($–NH_2$) groups in the molecule, and makes it possible to not only offer enough adsorption groups for increasing adsorption capacity toward dye but also improve the flocculation capacity of CMC for dye molecules. Moreover, CMC shows many unique properties, such as biocompatibility, biodegradation, biological activity, low toxicity and so on. Nevertheless, the cost of CMC is relatively higher.

Recently, clay materials are being widely considered as alternative low-cost adsorbents owing to they can be easily obtained. Among many kinds of clay minerals, montmorillonite (MMT) clay is the most commonly used adsorbent in the removal of organic pigments and dyes [22–24] due to their high surface area and high cation exchange capacity. Furthermore, many reports have been recently showed that the modified clays displayed higher adsorption capacity than the original clay [25,26].

The preparation of clay/polymer nanocomposites has attracted great attention because of their relative low production cost and remarkably improved mechanical and materials properties [27]. In our previous study [28], chitosan/montmorillonite (CTS–MMT) nanocomposite with the molar ratio of CTS to MMT of 5:1 showed good adsorption ability for CR dye. Moreover, as to our knowledge, the incorporation of *N*,*O*-CMC into MMT has not been studied and there is no literature focusing on the adsorption capacity of CR dye onto *N*,*O*-CMC–MMT nanocomposite. Therefore, in order to further enhance the adsorption capacity of nanocomposite, a novel *N*,*O*-CMC–MMT nanocomposite was synthesized and characterized, and the adsorption capacities for CR dye onto *N*,*O*-CMC–MMT nanocomposites were studied in this paper. Furthermore, the effects of the molar ratios of *N*,*O*-CMC and MMT, initial pH value in dye solution and adsorption temperature on the adsorption capacities of CR on the nanocomposite have been also investigated.

2. Experimental

2.1. Materials

The degree of deacetylation and a viscosity-average molecular weight of CTS (Zhejiang Yuhuan Ocean Biology Co., China) are 85% and 9.0×10^5, respectively. The cationic exchange capacity (CEC) of MMT (Shandong Longfeng Montmorillonite Co., China) is 102.8 mequiv./100 g. MMT was ground and sieved to 200 mesh size. Monochloroacetic acid was obtained from Tianjin Chemical Reagent Co., China. The molecular weight of CR (Tianjin Kermel Chemical Reagent Co., China) is 696.66 g/mol. Other agents used were all analytical grade and all solutions were prepared with distilled water.

2.2. Preparation of N,O-CMC–MMT nanocomposites

2.2.1. Preparation of N,O-CMC

CTS (5.00 g) was added to a 20 wt% sodium hydroxide solution (50.00 mL) for 12 h at room temperature, and then separated by filtration. The treated CTS was dipped into 50 mL of anhydrous alcohol in a three-necked flask by stirring for 30 min at room temperature, then monochloroacetic acid (3.58 g) was added into the reaction mixture and stirred for additional 30 min. Then the mixture was heated to 20 °C and allowed to continue for 1 h. Finally, the resultant solution was filtered and the filter cake dissolved in distilled water. The solution obtained was adjusted to pH 7.0 and precipitated by pouring into anhydrous alcohol. The white precipitate was filtered, washed with 70% (v/v) ethanol for three times and anhydrous alcohol once, then dried under vacuum at 80 °C to obtain products. The degree of substitution (35.3%) of the sample was determined by using potentiometric titration [29].

2.2.2. Preparation of N,O-CMC–MMT

1.0 g of MMT was swelled by 100-mL distilled water. *N*,*O*-CMC solution (containing *N*,*O*-CMC amounts of 0.0185, 0.037, 0.185, 0.925, and 1.85 g) was prepared by dissolving *N*,*O*-CMC in distilled water, and then the pH of the resulting solution was adjusted to 8.0 with 20 wt% NaOH solution, then *N*,*O*-CMC solution was slowly added to MMT suspension followed by stirring at 60 °C for 6 h to obtain the nanocomposites with *N*,*O*-CMC to MMT molar ratios of 1:10, 1:5, 1:1, 5:1 and 10:1, respectively. The formed composites were washed with distilled water until the pH of the supernatant reached 7.00, and then dried at 60 °C for 12 h. All samples as adsorbents were ground and sieved to 200 mesh size.

2.3. Adsorption experiments

All batch experiments were performed on a thermostated shaker (THZ-98A) with a shaking of 120 rpm. The effect of the molar ratios of *N*,*O*-CMC to MMT on dye removal was carried out in 25.00 mL of dye solutions (200 mg/L, initial pH 7.5) with 0.05 g of adsorbent at 30 °C for 480 min, respectively. The influence of pH on CR removal was studied by adjusting CR solutions (300 mg/L) to different pH values (4.0, 5.0, 6.0, 7.0, 8.0 and 9.0) using a pH meter (DELTA-320) and agitating 25.00 mL of dye solution with 0.05 g of adsorbent at 30 °C for 480 min. The effect of temperature on dye removal was carried out in 25.00 mL of dye solutions (300 mg/L, pH 7.0) with 0.05 g of adsorbent until equilibrium was established.

For kinetic study, 300 mg/L dye solutions (25.00 mL, pH 7.0) were agitated with 0.05 g of adsorbent at 30 °C for predetermined intervals of time, respectively. Batch equilibrium adsorption experiments were carried out by agitating 25.00 mL various dye concentrations of CR solution at pH 7.0 with 0.05 g of adsorbent at 30 °C for 480 min, respectively.

After a shaking time was completed, the suspension was separated from the adsorbent by centrifugation at 4500 rpm for 10 min. The absorbencies of dye solution were measured using a UV–vis spectrophotometer (Specord 200) at wavelength 500 nm (CR has a maximum absorbency at wavelength 500 nm on a UV–vis spectrophotometer. The molecular structure of CR is shown in Fig. 1). Then the concentrations of the dye solutions were determined by using linear regression equation ($y = 0.0342x + 0.0698$, $R^2 = 0.9999$) obtained by plot-

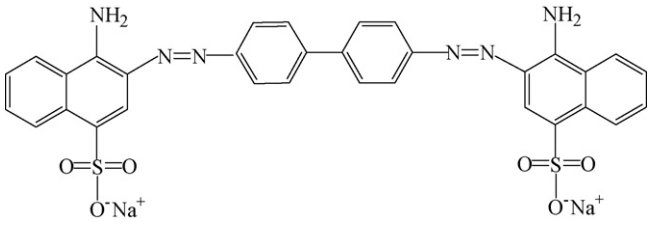

Fig. 1. Structure of CR (molecular formula: $C_{32}H_{22}N_6O_6S_2Na_2$).

ting a calibration curve for dye over a range of concentrations. The amounts of CR adsorbed onto samples were calculated by subtracting the final solution concentration from the initial concentration of dye solutions.

2.4. Characterization

The surface area and pore size of the samples were measured using an Accelerated Surface Area and Porosimetry System (Micromeritics, ASAP 2010) by BET-method at 76 K. IR spectra of the samples were characterized using a FTIR Spectrophotometer (Thermo Nicolet, NEXUS, TM) in KBr pellets. XRD analyses of the powdered samples were performed using an X-ray powder diffractometer with Cu anode (PANalytical Co. X'pert PRO), running at 40 kV and 30 mA, scanning from 4° to 18° at 3°/min. Micrographs of the samples were taken using an SEM (JSM-5600LV, JEOL Ltd.). Before observation of SEM, all samples were fixed on aluminum stubs and coated with gold.

3. Results and discussion

3.1. IR analysis of the nanocomposites

Fig. 2 shows IR spectra of MMT (a), three nanocomposites with the molar ratios of *N*,*O*-CMC to MMT 1:5 (b), 1:1 (c), 5:1 (d), and *N*,*O*-CMC (e). Compared with the IR spectra of MMT (a), Fig. 2 shows the adsorption band at 3442 cm^{-1}, corresponding to –OH stretching vibration of H_2O of MMT, strengthened and shifted to lower wave number 3430 cm^{-1} (Fig. 2b), 3428 cm^{-1} (Fig. 2c) and 3424 cm^{-1} (Fig. 2d). This suggests the vibration bands in *N*,*O*-CMC (O–H and N–H stretching, 3423 cm^{-1}) overlap with the bands of MMT (–OH stretching of H_2O). The characteristic absorption bands of the symmetric and asymmetric stretching vibrations of the $–CH_2$ (2885 cm^{-1}) and $–CH_3$ (2921 cm^{-1}) of intercalated *N*,*O*-CMC were observed on the IR spectra of *N*,*O*-CMC–MMT (Fig. 2b–d) and the intensity of the both adsorption bands increased with increasing the molar ratio of *N*,*O*-CMC to MMT. In addition, the adsorption band at 1636 cm^{-1}, assigned to –OH bending vibration of H_2O of the MMT, strengthened and shifted to lower wave number 1629 cm^{-1} (Fig. 2d), which indicates the $–COO^-$ group asymmetric stretching vibration of intercalated *N*,*O*-CMC (1600 cm^{-1}) overlapping with –OH bending vibration of H_2O of the MMT. At the same time, the $–COO^-$ group symmetric stretching vibration (1417 cm^{-1}) and the second –OH group stretching vibration (1086 cm^{-1}) of intercalated *N*,*O*-CMC were observed on the IR spectra of *N*,*O*-CMC–MMT (Fig. 2d) with increasing the molar ratio of *N*,*O*-CMC to MMT. The information observed from IR spectra indicates that the molar ratio of *N*,*O*-CMC to MMT could influence chemical environment of the nanocomposites and then may have an influence on absorption properties of the nanocomposites, which will be discussed in the following sections in detail.

3.2. X-ray diffraction analysis of the nanocomposites

X-ray diffraction (XRD) is an effective method for the investigation of the intercalation existence of montmorillonite. Fig. 3 shows that the XRD patterns of MMT (a) and three nanocomposites with the molar ratios of *N*,*O*-CMC to MMT of 1:5 (b), 1:1 (c) and 5:1 (d). The XRD pattern of MMT shows a typical diffraction peak at 6.94°, corresponding to a basal spacing of 12.74 Å. After intercalation with *N*,*O*-CMC, this peak shifts to lower angle and even disappears. When the molar ratio of *N*,*O*-CMC to MMT is 1:5, there is a diffraction peak is at 5.78° ($d = 1.53$ nm), which means that the intercalation has occurred and the intercalated nanocomposite have been formed. With the molar ratio of *N*,*O*-CMC to MMT increases to 5:1, the peak nearly disappears. This indicates the disordered intercalated or exfoliated structure in

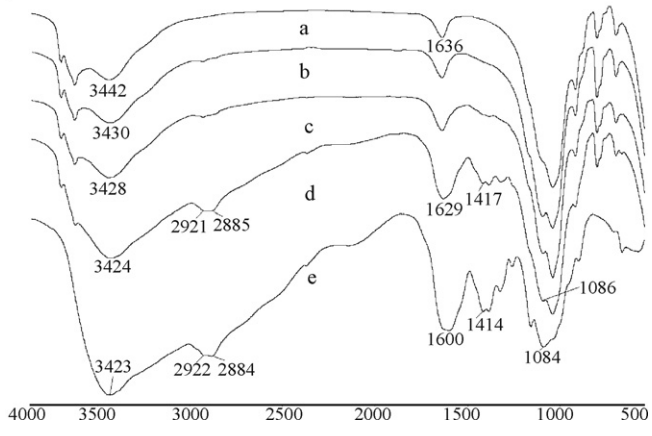

Fig. 2. IR spectra of the MMT (a), the nanocomposites with the molar ratios *N*,*O*-CMC to MMT of 1:5 (b), 1:1 (c), 5:1 (d) and *N*,*O*-CMC (e).

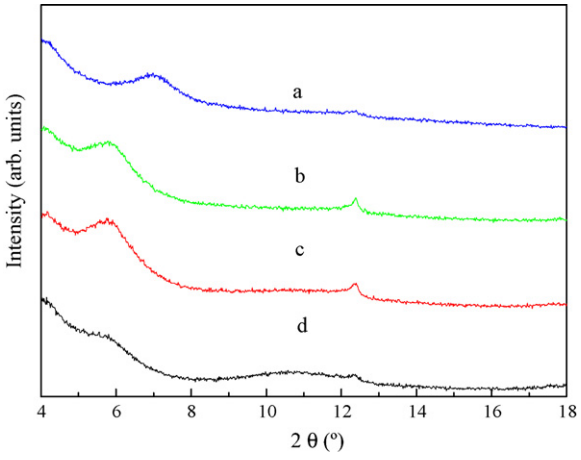

Fig. 3. XRD powder patterns of the MMT (a), the nanocomposites with the molar ratios of *N*,*O*-CMC to MMT of 1:5 (b), 1:1 (c) and 5:1 (d).

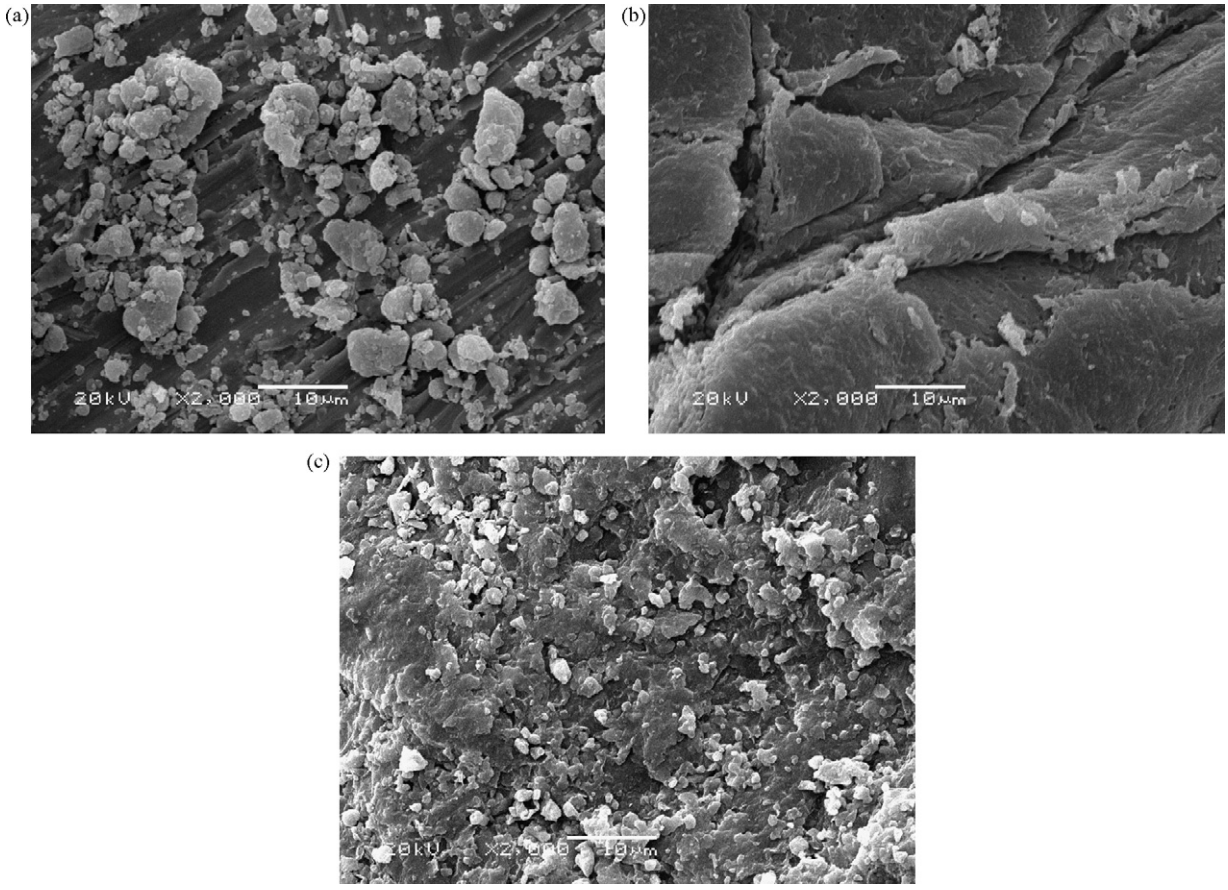

Fig. 4. SEM images of the MMT (a), *N*,*O*-CMC (b) and *N*,*O*-CMC–MMT nanocomposite (c).

N,*O*-CMC–MMT nanocomposite. According to the results of XRD and FTIR, it can be concluded that almost all *N*,*O*-CMC intercalated into MMT interlayer with destroying the crystalline structure of MMT.

3.3. SEM images analysis of the nanocomposites

Fig. 4 shows the SEM images of MMT (a), *N*,*O*-CMC (b) and *N*,*O*-CMC–MMT nanocomposite (c). It can be seen that after intercalation with *N*,*O*-CMC, MMT particles are uniformly distributed in the matrix structure of *N*,*O*-CMC and do not give an indication of aggregation (Fig. 4c). Furthermore, the fact that the dimension of MMT becomes smaller compared with the initial particle size suggests that the disordered intercalated or exfoliated structure in *N*,*O*-CMC–MMT nanocomposite, is in agreement with the results of XRD patterns.

3.4. Effect of molar ratios of N,O-CMC to MMT of the nanocomposites on adsorption

N,*O*-CMC–MMT mixtures tend to shrink with increasing of the molar ratios of *N*,*O*-CMC to MMT, which enhances the agglomerate capability *N*,*O*-CMC–MMT and facilitates the separation of the adsorbents from the solution. The effect of molar ratios of *N*,*O*-CMC to MMT of the nanocomposites on adsorption capacities of *N*,*O*-CMC–MMT nanocomposites is shown in Fig. 5. It can be seen that the adsorption capacities of the nanocomposites increase with the increase of the molar ratio of *N*,*O*-CMC to MMT till reaching a maximum at 5:1, and increase hardly with further increase of the molar ratio of *N*,*O*-CMC to MMT. It may be explained by the following two reasons: on the one hand, the amounts of active hydroxyl (–OH), carboxyl (–COOH) and amine ($–NH_2$) groups increase with increasing

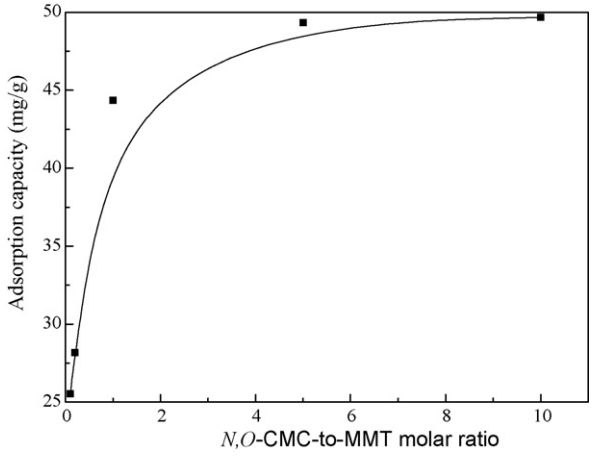

Fig. 5. Effect of the molar ratios of *N*,*O*-CMC to MMT on adsorption capacity of the nanocomposites for CR. Adsorption experiments—dye concentration: 200 mg/L; sample dose: 0.05 g/25.00 mL; initial pH 7.5; temperature: 30 °C; equilibrium time: 480 min.

Table 1
The specific surface areas and the average pore size of *N*,*O*-CMC–MMT nanocomposites

Samples	Specific surface area (m^2/g)	Average pore size (nm)
MMT	61.4	6.7
Nanocomposite with the molar ratio of *N*,*O*-CMC to MMT of 1:5	41.6	7.6
Nanocomposite with the molar ratio of *N*,*O*-CMC to MMT of 1:1	29.2	8.7
Nanocomposite with the molar ratio of *N*,*O*-CMC to MMT of 5:1	15.9	12.1

of the molar ratio of *N*,*O*-CMC to MMT, which result in an increase in adsorption capacities of CR on *N*,*O*-CMC–MMT. On the other hand, the introduction of *N*,*O*-CMC in the MMT galleries can improve the flocculation capacity of MMT and increase adsorption capacity of *N*,*O*-CMC–MMT for CR. However, the adsorption capacities increase hardly when the molar ratio of *N*,*O*-CMC to MMT exceeds 5:1, which is attributed to the amount of intercalated *N*,*O*-CMC is saturated.

To further support the explanation mentioned above, we also investigated the effect of molar ratio of *N*,*O*-CMC to MMT on the surface area and the average pore size of the nanocomposites. The test results indicate (see Table 1), compared with MMT (61.4 m^2/g), the surface area of the nanocomposites decreasing with increasing of the molar ratio of *N*,*O*-CMC to MMT from 1:5 (41.6 m^2/g) to 5:1 (15.9 m^2/g). These are attributed to most of the exchange sites of MMT satisfied by *N*,*O*-CMC species with large molecular size and the inaccessibility of the internal surface to nitrogen gas [25]. However, the average pore size of the nanocomposites increase with increasing of the molar ratio of *N*,*O*-CMC to MMT from 1:5 (7.6 nm) to 5:1 (12.1 nm) by comparing with MMT (6.7 nm). These results show that the larger average pore size may facilitate an increase of CR dye adsorption on *N*,*O*-CMC–MMT and the synergic effects of these factors such as the changes in the crystalline structure (it also can be seen from Figs. 2–4), the BET surface area and the average pore size may result in the higher adsorption capacity of *N*,*O*-CMC–MMT with the molar ratios of *N*,*O*-CMC to MMT of 5:1. Therefore, the following discussion will be focused on *N*,*O*-CMC–MMT with the molar ratios of *N*,*O*-CMC to MMT of 5:1 in this study.

3.5. Effect of pH values on adsorption

The pH is the most important factor affecting the adsorption process. The effect of pH value in the original solution on adsorption capacity of *N*,*O*-CMC–MMT nanocomposite was investigated and shown in Fig. 6. CR dye is slightly soluble in water with a pH value of 2.0, so the range of pH for CR adsorption test selected in this study was between 4.0 and 9.0. The adsorption capacity of CR on *N*,*O*-CMC–MMT decreased from 96.61 mg/g to 73.48 mg/g with increasing pH from 4.0 to 7.0, slowly reduced from 73.48 mg/g to 67.47 mg/g with further increasing pH from 7.0 to 9.0. It was observed that the adsorption is highly dependent on the pH of the solution, which affects the surface charge of the adsorbent and the degree of ionization and speciation of the adsorbate. At lower pH more protons will be available, therefore increasing electrostatic attraction between negatively charged dye anions and positively charged adsorption sites and causing an increase in dye adsorption [30]. The high adsorption capacity is due to the strong electrostatic interaction between the positive surfaces of *N*,*O*-CMC and CR dye anions. At pH above 7.0, the repulsion between anionic dye molecules and the excessive hydroxyl ions results in a sharp decrease in adsorption. However, the significant adsorption of the anionic dye on the adsorbent still occurred at pH above 7.0 due to the fact that a chemical interaction between CR dye and *N*,*O*-CMC–MMT takes place. A similar trend of pH effect was observed for the adsorption of CR dye onto wollastonite [31], biogas waste slurry [32], banana pith [33], waste Fe(III)/Cr(III) hydroxide [34], waste orange peel [35], waste red mud [36] and activated carbon [37].

3.6. Effect of temperature on adsorption

The effect of temperature on adsorption capacity of *N*,*O*-CMC–MMT nanocomposite is shown in Fig. 7. As can be seen, the adsorption capacity of nanocomposite sharply increased from 73.66 mg/g to 91.82 mg/g with increase of temperature from 30 °C to 40 °C, and slowly increased 91.82 mg/g to 95.21 mg/g with further increase of temperature from 40 °C to 50 °C. The phenomenon indicated that high-temperature facilitated to adsorption of CR dye on *N*,*O*-CMC–MMT nanocomposite. It is well known that increasing temperature may produce a swelling effect within the internal structure of absorbent, penetrating the large dye molecule further [38]. However, the mobility of the large dye ions increase with increas-

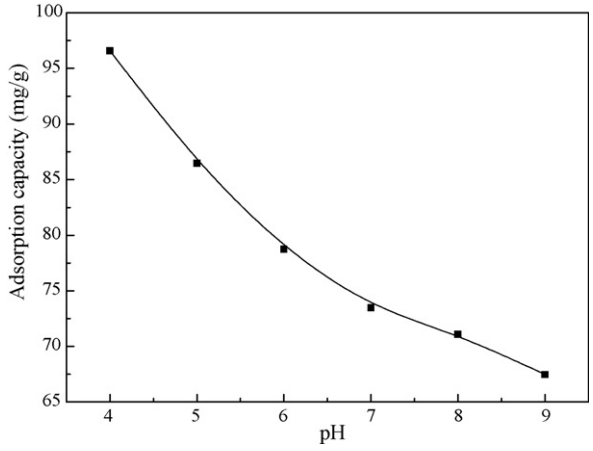

Fig. 6. Effect of the pH values on adsorption capacity of *N*,*O*-CMC–MMT nanocomposite for CR. Adsorption experiments—dye concentration: 300 mg/L; sample dose: 0.05 g/25.00 mL; pH range: 4.0–9.0; temperature: 30 °C; equilibrium time: 480 min.

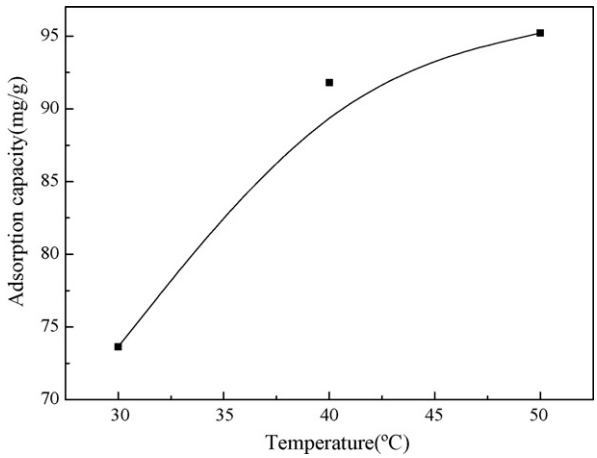

Fig. 7. Effect of the temperature on adsorption capacity of *N*,*O*-CMC–MMT nanocomposite for CR. Adsorption experiments—dye concentration: 300 mg/L; sample dose: 0.05 g/25.00 mL; pH: 7.0; temperature: 30–50 °C; equilibrium time: 480 min.

ing temperature, which leads a slow increase in the adsorption capacity of nanocomposite with further increasing temperature. A similar behavior has been reported for the adsorption of CR on activated carbon prepared from coir pith [37] and calcium-rich fly ash [9].

3.7. Adsorption kinetics

The effect of adsorption time on adsorption capacities of *N*,*O*-CMC–MMT nanocomposites was investigated and the results are shown in Fig. 8. It can be seen from Fig. 8 that adsorption capacity of *N*,*O*-CMC–MMT nanocomposite sharply increased with 120 min, 120 min later, and gradually increased with prolonging the contact time until equilibrium. Under our experimental conditions, the equilibrium time for the adsorption of CR on *N*,*O*-CMC–MMT is 480 min.

In order to investigate the adsorption processes of CR on the adsorbents, pseudo-first-order and pseudo-second-order kinetic models were used.

The pseudo-first-order equation [39] can be expressed as

$$\log(q_e - q_t) = \log q_e - \frac{k_1 t}{2.303} \quad (1)$$

The pseudo-second-order model [40] is given as

$$\frac{t}{q_t} = \frac{1}{k_2 q_e^2} + \frac{t}{q_e} \quad (2)$$

where q_e and q_t are the amounts of adsorption dye (mg/g) at equilibrium and at time t (min), k_1 (min^{-1}) and k_2 ($g\,mg^{-1}\,min^{-1}$) are the adsorption rate constant of pseudo-first-order, pseudo-second-order adsorption, respectively. The linear plots of $\log(q_e - q_t)$ versus t and (t/q_t) versus t are drawn for the pseudo-first-order and the pseudo-second-order models, respectively. The rate constants k_1 and k_2 can be obtained from the plot of experimental data.

The correlation coefficients (R) of the pseudo-first-order and the pseudo-second-order models are 0.9997 and 0.9745 for the nanocomposite, respectively. It can be seen that the adsorption of CR is in good agreement with pseudo-second-order model rather than pseudo-first-order model. These results indicated that the adsorption rate of CR dye depends on the concentration of dye at the absorbent surface and the absorbance of these absorbed at equilibrium [41].

3.8. Adsorption isotherms

Fig. 9 shows the influence of initial dye concentration on adsorption capacity of *N*,*O*-CMC–MMT nanocomposite. It is clear that initial dye concentration is an important factor affecting adsorption capacity of the nanocomposite. As shown in Fig. 9, the adsorption capacities of the nanocomposite increased sharply from 48.71 mg/g to 73.60 mg/g with increase of dye concentration from 100 mg/L to 300 mg/L, and hardly increased with further increase in dye concentration.

The equilibrium adsorption data were interpreted using two isotherm equations, namely, the Langmuir [42] and the Fre-

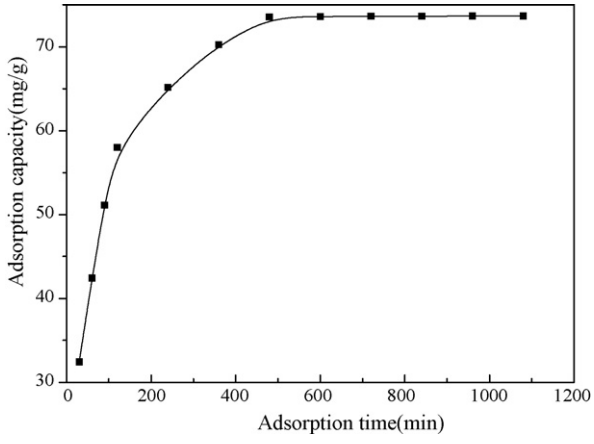

Fig. 8. Effect of the adsorption time on adsorption capacity of *N*,*O*-CMC–MMT nanocomposite for CR. Adsorption experiments—dye concentration: 300 mg/L; sample dose: 0.05 g/25.00 mL; pH: 7.0; temperature: 30 °C.

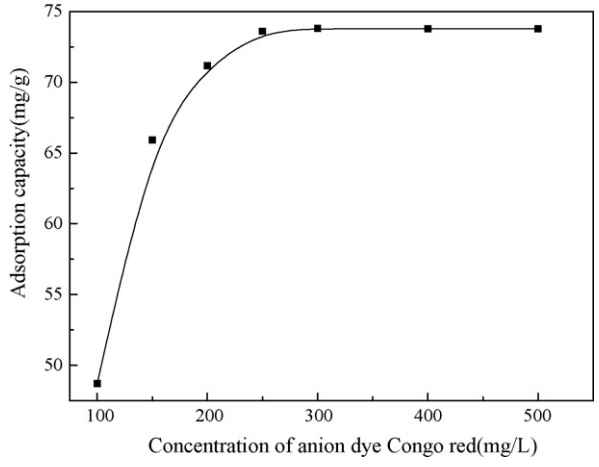

Fig. 9. Effect of the dye concentration on adsorption capacity of *N*,*O*-CMC–MMT nanocomposite for CR. Adsorption experiments—sample dose: 0.05 g/25.00 mL; pH: 7.0; temperature: 30 °C; equilibrium time: 480 min.

Table 2
The q_m values for the adsorption of CR on different adsorbents

Adsorbents	q_m (mg/g)	References
N,*O*-CMC–MMT	74.24	Our data in the paper
CTS–MMT	54.52	[28]
CTS powder	74.73	[28]
CTS bead	92.59	[16]
Waste Fe(III)/Cr(III) hydroxide	44.00	[34]
Waste orange peel	22.44	[35]
Waste banana pith	20.29	[33]
Biogas waste slurry	9.50	[32]
Waste red mud	4.05	[36]

undlich equations [43], which are represented by the following equations, respectively:

$$\frac{C_e}{q_e} = \frac{1}{bq_m} + \frac{C_e}{q_m} \quad (3)$$

$$q_e = K_f C_e^{1/n} \quad (4)$$

where q_m (mg/g) and b (L/mg) are Langmuir isotherm coefficients. The value of q_m represents the maximum adsorption capacity. K_f (mg/g) and n are Freundlich constants. Two adsorption isotherms were constructed by plotting the C_e/q versus C_e, $\log q$ versus $\log C_e$, respectively.

The values of R^2 of Langmuir and Freundlich models are 0.9999 and 0.9294, respectively. It can be concluded that the Langmuir isotherm best represents the equilibrium adsorption of CR on *N*,*O*-CMC–MMT nanocomposite, which suggests the monolayer coverage of the dye on the surface of nanocomposite. Similar behavior was also found for the adsorption of CR onto red mud [36], activated coir pith [37], and mesoporous-activated carbons [44]. The q_m values of CR on *N*,*O*-CMC–MMT were compared with those of other absorbents (see Table 2). It can be seen from Table 2 that the q_m value of *N*,*O*-CMC–MMT is larger than those of other absorbents such as CTS–MMT, waste orange peel, waste banana pith, and so on. CTS and CMC have relative higher adsorption capacity [16,28], however, the cost of CTS and CMC are relatively higher. Thus, *N*,*O*-CMC–MMT nanocomposite is useful as a promising adsorbent for the removal of CR dye in wastewater treatment.

4. Conclusion

Novel *N*,*O*-CMC–MMT nanocomposites were synthesized by intercalation reaction between *N*,*O*-CMC and MMT in distilled water. Adsorption tests of CR dye on *N*,*O*-CMC–MMT nanocomposites were carried out and the results obtained from this study show that the nanocomposite with the molar ratios of *N*,*O*-CMC to MMT of 5:1 exhibited the higher adsorption capacity. The kinetic and isotherm studies indicated that the pseudo-second-order model and the Langmuir model well described the adsorption equilibrium of CR on *N*,*O*-CMC–MMT nanocomposite. As a novel nanocomposite material, *N*,*O*-CMC–MMT is a promising biosorbent for dye removal from CR dye wastewater.

Acknowledgement

This work was financially supported with the science and technology major project of Gansu Province (No. 2GS052-A52-002-07).

References

[1] S.H. Lina, R.S. Juang, Y.H. Wang, Adsorption of acid dye from water onto pristine and acid-activated clays in fixed beds, J. Hazard. Mater. 113 (2004) 195–200.
[2] M.S. Chiou, G.S. Chuang, Competitive adsorption of dye metanil yellow and RB15 in acid solutions on chemically cross-linked chitosan beads, Chemosphere 62 (2006) 731–740.
[3] O.J. Hao, H. Kim, P.C. Chiang, Decolorization of wastewater, Crit. Rev. Environ. Sci. Technol. 30 (2000) 449–505.
[4] Y.M. Slokar, A. Majcen-Le Marechal, Methods of decoloration of textile wastewaters, Dyes Pigments 37 (1998) 335–356.
[5] W.T. Tsai, Y.M. Chang, C.W. Lai, C.C. Lo, Adsorption of basic dyes in aqueous solution by clay adsorbent from regenerated bleaching earth, Appl. Clay Sci. 29 (2005) 149–154.
[6] M. Arami, N.Y. Limaee, N.M. Mahmoodi, N.S. Tabrizi, Removal of dyes from colored textile wastewater by orange peel adsorbent: equilibrium and kinetic studies, J. Colloids Interf. Sci. 288 (2005) 371–376.
[7] A. Tor, Y. Cengeloglu, Removal of congo red from aqueous solution by adsorption onto acid activated red mud, J. Hazard. Mater. 138 (2006) 409–415.
[8] Z. Eren, F. Nuran, Equilibrium and kinetic mechanism for Reactive Black sorption onto high lime soma fly ash, J. Hazard. Mater. 143 (2007) 226–232.
[9] B. Acemioğlu, Adsorption of congo red from aqueous solution onto calcium-rich fly ash, J. Colloids Interf. Sci. 274 (2004) 371–379.
[10] S.B. Wang, Y. Boyjoo, A. Choueib, Z.H. Zhu, Removal of dyes from aqueous solution using fly ash and red mud, Water Res. 39 (2005) 129–138.
[11] K.P. Singh, D. Mohan, S. Sinha, G.S. Tondon, D. Gosh, Color removal from wastewater using low-cost activated carbon derived from agricultural waste material, Ind. Eng. Chem. Res. 42 (2003) 1965–1976.
[12] Y.P. Guo, J.Z. Zhao, H. Zhang, S.F. Yang, J.R. Qi, Z.C. Wang, H.D. Xu, Use of rice husk-based porous carbon for adsorption of Rhodamine B from aqueous solutions, Dyes Pigments 66 (2005) 123–128.
[13] A. Bhatnagar, A.K. Jain, A comparative adsorption study with different industrial wastes as adsorbents for the removal of cationic dyes from water, J. Colloids Interf. Sci. 281 (2005) 49–55.
[14] S. Wang, H. Li, Dye adsorption on unburned carbon: kinetics and equilibrium, J. Hazard. Mater. 126 (2005) 71–77.
[15] H. Aydına, G. Baysalb, Adsorption of acid dyes in aqueous solutions by shells of bittim (Pistacia khinjuk Stocks), Desalination 196 (2006) 248–259.
[16] S. Chatterjee, S. Chatterjee, B.P. Chatterjee, A.K. Guha, Adsorptive removal of congo red, a carcinogenic textile dye by chitosan hydrobeads: binding mechanism, equilibrium and kinetics, Colloids Surf. A: Physicochem. Eng. Aspects 299 (2007) 146–152.
[17] F.C. Wu, R.L. Tseng, R.S. Juang, Comparative adsorption of metal and dye on flake- and bead-types of chitosans prepared from fishery wastes, J. Hazard. Mater. 73 (2000) 63–75.
[18] M.S. Chiou, H.Y. Li, Adsorption behavior of reactive dye in aqueous solution on chemical cross-linked chitosan beads, Chemosphere 50 (2003) 1095–1105.
[19] X. Zeng, E. Ruckenstein, Membrane chromatography: preparation and applications to protein separation, Biotechnol. Prog. 15 (1999) 1003–1019.
[20] Z. Jia, D. Shen, W. Xu, Synthesis and antibacterial activities of quaternary ammonium salt of chitosan, Carbohydr. Res. 333 (2001) 1–6.
[21] Z.P. Zhao, Z. Wang, N. Ye, S.C. Wang, A novel *N*,*O*-carboxymethyl amphoteric chitosan/poly(ethersulfone) composite MF membrane and its charged characteristics, Desalination 144 (2002) 35–39.
[22] A.H. Gemeay, A.S. EI-Sherbiny, A.B. Zaki, Adsorption and kinetic studies of the intercalation of some organic compounds onto Na^+-montmorillonite, J. Colloids Interf. Sci. 245 (2002) 116–125.

[23] N. Miyamoto, R. Kawai, K. Kuroda, M. Ogawa, Adsorption and aggregation of a cationic cyanime dye on layered clay minerals, Appl. Clay Sci. 16 (2000) 161–170.
[24] A.H. Gemeay, Adsorption characteristics and the kinetics of cation exchange of rhodamine 6G with Na^+-montmorillonite, J. Colloids Interf. Sci. 251 (2002) 235–241.
[25] C.C. Wang, L.C. Juang, T.C. Hsu, C.K. Lee, J.F. Lee, F.C. Huang, Adsorption of basic dyes onto montmorillonite, J. Colloids Interf. Sci. 273 (2004) 80–86.
[26] A.S. Özcan, A. Özcan, Adsorption of acid dyes from aqueous solutions onto acid-activated bentonite, J. Colloids Interf. Sci. 276 (2004) 39–46.
[27] S.S. Ray, M. Okamoto, Polymer/layered silicate nanocomposites: a review from preparation to processing, Prog. Polym. Sci. 28 (2003) 1539–1641.
[28] L. Wang, A.Q. Wang, Adsorption characteristics of congo red onto the chitosan/montmorillonite nanocomposite, J. Hazard. Mater. 147 (2007) 979–985.
[29] S.J. Lu, X. Song, D. Cao, Preparation of water-soluble chitosan, J. Appl. Polym. Sci. 91 (2004) 3497–3503.
[30] A.S. Özcan, B. Erdem, A. Özcan, Adsorption of Acid Blue 193 from aqueous solutions onto Na–bentonite and DTMA–bentonite, J. Colloids Interf. Sci. 280 (2004) 44–54.
[31] V.N. Singh, G. Mishra, K.K. Panday, Removal of congo red by wollastonite, Indian J. Technol. 22 (1984) 70–71.
[32] C. Namasivayam, R.T. Yamuna, Removal of congo red from aqueous solutions by biogas waste slurry, J. Chem. Technol. Biotechnol. 53 (1992) 153–157.
[33] C. Namasivayam, N. Kanchana, Waste banana pith as adsorbent for colour removal from wastewaters, Chemosphere 25 (1992) 1691–1705.
[34] C. Namasivayam, R. Jeyakumar, R.T. Yamuna, Dye removal from wastewater by adsorption on waste Fe(III)/Cr(II1) hydroxide, Waste Manage. 14 (1994) 643–648.
[35] C. Namasivayam, N. Muniasamy, K. Gayathri, M. Rani, K. Ranganathan, Removal of dyes from aqueous solutions by cellulosic waste orange peel, Bioresour. Technol. 57 (1996) 37–43.
[36] C. Namasivayam, D.J.S.E. Arasi, Removal of congo red from wastewater by adsorption onto waste red mud, Chemosphere 34 (1997) 401–417.
[37] C. Namasivayam, D. Kavitha, Removal of congo red from water by adsorption onto activated carbon prepared from coir pith, an agricultural solid waste, Dyes Pigments 54 (2002) 47–58.
[38] K.G. Bhattacharyya, A. Sarma, Adsorption characteristics of the dye, brilliant green, on neem leaf powder, Dyes Pigments 57 (2003) 211–222.
[39] S. Lagergren, About the theory of so-called adsorption of soluble substances, Kungliga Svenska Vetenskapsakademiens, Handlingar 24 (1898) 1–39.
[40] Y.S. Ho, G. McKay, Pseudo-second order model for sorption processes, Process Biochem. 34 (1999) 451–465.
[41] S.L. Sun, A.Q. Wang, Adsorption kinetics of Cu(II) ions using *N*,*O*-carboxymethyl-chitosan, J. Hazard. Mater. 131 (2006) 103–111.
[42] I. Langmuir, The adsorption of gases on plane surfaces of glass, mica and platinum, J. Am. Chem. Soc. 40 (1918) 1361–1403.
[43] H.M.F. Freundlich, Uber die adsorption in lasungen, Z. Phys. Chem. 57 (1906) 385–470.
[44] E.L. Grabowska, G. Gryglewicz, Adsorption characteristics of congo red on coal-based mesoporous activated carbon, Dyes Pigments 74 (2007) 34–40.